Applied Catalysis B: Environmental 129 (2013) 137–145

Contents lists available at SciVerse ScienceDirect

Applied Catalysis B: Environmental

journal homepage: www.elsevier.com/locate/apcatb

Citric acid loading for MoS_2-based catalysts supported on SBA-15. New catalytic materials with high hydrogenolysis ability in hydrodesulfurization

Diego Valencia*, Tatiana Klimova

Facultad de Química, Universidad Nacional Autónoma de México, Cd. Universitaria, Coyoacán, México D.F., 04510, Mexico

ARTICLE INFO

Article history:
Received 20 June 2012
Received in revised form 6 September 2012
Accepted 7 September 2012
Available online 16 September 2012

Keywords:
Hydrodesulfurization
SBA-15
Citric acid
Dibenzothiophene
Carbon

ABSTRACT

The aim of this work is to get a deeper insight into the effect of citric acid (CA) loading in NiMo sulfided catalysts supported on SBA-15 on their behavior in hydrodesulfurization (HDS). Catalysts were prepared by simultaneous impregnation of Ni, Mo and CA species, varying the CA amount in aqueous solution. After the impregnation, NiMoCA catalysts were dried at 100 °C under air atmosphere without calcination. Catalysts were characterized by several techniques (TGA, N_2 physisorption, small-angle and powder XRD, FT-IR, UV–vis DRS, TPR, elemental analysis and HRTEM) and tested in HDS of dibenzothiophene (DBT). N_2 physisorption, small-angle XRD and FT-IR showed the adsorption of CA on the SBA-15 surface. XRD characterization demonstrated that Ni and Mo oxide species were well dispersed in all catalysts. UV–vis DRS revealed better dispersion of Mo species with the increase of CA loading. TPR experiments exhibited an important effect of CA under reducing atmosphere; it can be reduced to leave carbon on the catalytic materials. This observation was confirmed by carbon analysis which showed an increase in the amount of carbon in the same direction than the CA loading. HDS of DBT showed differences in activity and selectivity of the catalysts prepared with different CA loading. We observed outstanding promotion of direct desulfurization (DDS) route with increasing the CA amount. The preference of DBT to react over NiMoCA catalysts toward DDS route was an unexpected behavior.

© 2012 Elsevier B.V. All rights reserved.

1. Introduction

Since oil-based fuels will continue to be an essential component for generating power, there is a clear motivation to produce cleaner fuels to diminish atmospheric pollution of certain toxic emissions. Gasoline and diesel with large amounts of S have serious problems to be used without pretreatment. The industrial process to diminish the S content in fuels is called hydrodesulfurization (HDS). In this process, a fluid phase containing hydrocarbons reacts with H_2 in presence of a heterogeneous catalyst at high pressure and temperature. This process aims to reduce the sulfur content below 15 ppm in diesel, imposed by various environmental regulations [1].

Many efforts are aimed to design more active and/or selective HDS catalysts, depending on their particular application. It is known that the active phases of the HDS catalysts are the MoS_2 or WS_2 nanocrystallites promoted by cobalt or nickel, deposited on a high specific surface area supports. Catalytic behavior of HDS catalysts depends on a series of factors and their combinations (active phase, promoter and support). Using new supports with appropriate physicochemical properties, e.g., dispersion of active phase, large surface area, thermal and mechanical resistance are an attractive option for new catalyst design. Mesostructured materials such as MCM-41, SBA-15, KIT-6 have been used for NiMo and CoMo HDS catalysts with good results [2,3]. Some of these silica-based supports have been modified with P, Al, Ti and Zr to increase the activity and selectivity of NiMo and CoMo HDS catalysts [4–7].

New MoS_2-based catalytic materials have been synthesized with modifications in their textural properties and chemical composition with important increasing in HDS activity [2–7]. Another possibility to enhance the catalytic activity of new materials is the use of new Ni or Mo aqueous solution precursors that were impregnated to support. For instance, chelating agents are an attractive alternative for preparing HDS catalysts which could be able to reduce the S content in fuels. Chelating agents such as citric acid (CA), 1,2-cyclohexanediamine-N,N,N',N'-tetraacetic acid (CyDTA) and nitriloacetic acid (NTA) resulted in high active catalysts for HDS [8–10].

The use of chelating agents has some implications in (i) liquid phase: metal speciation in aqueous solution is dependent of metal, chelating agents concentrations and pH of solution, these experimental conditions allow the formation of stable coordination compounds [11,12]; (ii) liquid–solid interface: interaction between metals and support has changes due to surface charge of support at distinct pH, stability of coordination compounds results in chelating agents affinity and their easy or difficult replacement by support [13,14], and (iii) properties of materials: morphology

* Corresponding author.
E-mail address: dvalencia@comunidad.unam.mx (D. Valencia).

0926-3373/$ – see front matter © 2012 Elsevier B.V. All rights reserved.
http://dx.doi.org/10.1016/j.apcatb.2012.09.006

of active phase, dispersion of metal oxides in the support and the promotion of highly active phases [15–18].

The chelating agent structure is important to synthesize new catalytic materials. CA has been used in the preparation of MoS_2-based catalysts for deep HDS. CA for preparing HDS catalysts is a great alternative because of its low cost, non-toxic products, easy manipulation and formation of stable coordination compounds in aqueous solution [19,20]. CoMoCA catalyst supported on HY-Al_2O_3 exhibited high activity in deep HDS of Middle East straight run gas oil (SRLGO) containing 1.33 wt.% sulfur. This catalyst removed sulfur below 16 ppm and presented some advantages, e.g., resistance to the presence of N-containing compounds reaching elimination of N from 260 ppm below 5 ppm at 350 °C [21,22]. The optimal temperature for the thermal treatment of this catalyst before sulfidation stage was up to 100 °C. The rate constants decreased at higher temperatures (between 300 and 500 °C) [23]. NiMo catalysts were prepared with different amounts of CA and supported on ZrO_2–TiO_2. These catalysts were impregnated at acidic pH, and they were sulfided without previous calcination. The best activity results in HDS of dibenzothiophene (DBT) were obtained when the Ni:CA molar ratio was 1:2, although no selectivity modification was observed for any molar ratio [24]. NiW catalysts supported on Al_2O_3 were prepared with CA to get a deeper insight into the effect of this organic acid during the preparation of HDS catalysts. They exhibited high catalytic activity in HDS of 4,6-dimethyldibenzothiophene (4,6-DMDBT). It was observed important modifications of the metal–support interactions by carbon incorporation from CA on the alumina surface [25]. Carbon in HDS catalysts modifies the external structure of the active phase, substitution of S by C is thermodynamically unfavorable. The Mo—S bond is more stable than Mo—C bond in activation conditions of catalysts [26]. In our previous work, we reported an important effect of CA addition in the activity and selectivity of NiMo/SBA-15 catalysts depending on thermal treatment and pH of impregnation solutions. We noted that CA could act as a carbon source [27].

In this work, we used SBA-15 mesoporous material as a support for NiMo sulfided catalysts and CA as chelating agent in impregnation solutions. We prepared a series of NiMoCA(x) catalysts supported on SBA-15, where x is the amount of CA in aqueous solution to understand the effect of CA loading on the behavior of these catalysts in HDS of DBT.

2. Experimental

2.1. Preparation of catalysts

SBA-15 was prepared according to the previously procedure [28,29] using the triblock copolymer P123 (M_{av} = 5800, $EO_{20}PO_{70}EO_{20}$, Aldrich) as the structure-directing agent and tetraethyl orthosilicate (TEOS, Aldrich, 99.999%) as the silica source. P123 copolymer (4 g) was dissolved in water (30 g) and 2 M HCl (120 g) solution at 35 °C. Then TEOS (8.5 g) was added into the solution. The mixture was stirred at 35 °C for 20 h and then aged at 80 °C for 48 h without stirring. The solid product was recovered by filtration, washed with deionized water and air-dried at room temperature. Calcination was carried out in static air at 550 °C for 6 h.

NiMo catalysts supported on SBA-15 were prepared by a standard incipient wetness coimpregnation technique reported [30]. The calcined support was co-impregnated using aqueous solutions of ammonium heptamolybdate, $(NH_4)_6Mo_7O_{24}{\cdot}4H_2O$ (Merck, 99%), nickel nitrate, $Ni(NO_3)_2{\cdot}6H_2O$ (Baker), and citric acid, $C_6H_8O_7{\cdot}H_2O$ (Merck, 99.5%) at pH 9, pH was adjusted with ammonia solution. NiMoCA(x) catalysts supported on SBA-15 were impregnated with different amounts of CA in impregnation solution, the molar ratio was Ni:Mo:CA = 1:2.1:x, (where x = 2.7, 4.2, 6.3, 7.4). After co-impregnation, catalysts were thermal treated at 100 °C for 12 h in static air atmosphere, this temperature was used to maintain the CA in catalyst until activation stage. The nominal compositions of the catalysts were 12 wt.% of MoO_3 and 3 wt.% of NiO.

2.2. Characterization of catalysts

The catalysts were characterized by termogravimetric analysis (TGA), N_2 physisorption, small-angle and powder X-ray diffraction (XRD), infrared spectroscopy (FT-IR), UV–vis diffuse reflectance spectroscopy (DRS), temperature-programmed reduction (TPR), elemental analysis and high resolution transmission electron microscopy (HRTEM). TGA experiments of dried samples were performed on a Mettler-Toledo TGA/SDTA 851^e, under static air atmosphere using a heating rate of 10 °C/min from 40 to 1000 °C. N_2 adsorption–desorption isotherms were measured with a Micromeritics ASAP 2000 automatic analyzer at liquid N_2 temperature. Prior to the experiments, the samples were degassed ($p < 10^{-1}$ Pa) at 100 °C for 6 h. Specific surface areas were calculated by the BET method (S_{BET}), the total pore volume (V_p) was determined by nitrogen adsorption at a relative pressure of 0.98 and pore size distributions from the desorption isotherms by the BJH method. The mesopore diameter (D_P) corresponds to the maximum of the pore size distribution. The micropore area (S_μ) was estimated using the correlation of t-Harkins & Jura (t-plot method). Small-angle XRD (2Θ = 1–10°) was performed on a Bruker D8 Advance diffractometer using small divergence and scattering slits of 0.05°. The a_o unit-cell parameter was estimated from the position of the (1 0 0) diffraction line ($a_o = d_{100} \times 2/\sqrt{3}$) [31]. XRD patterns were recorded in the $3° \leq 2\Theta \leq 70°$ range on a Siemens D5000 diffractometer, using Cu Kα radiation (λ = 1.5406 Å) and a goniometer speed of 1° (2Θ) min^{-1}. FT-IR spectra of the support and catalysts were recorded in a transmittance mode with a Varian 640-IR FT-IR spectrophotometer. UV–vis electronic spectra of the samples were recorded in the wavelength range 200–800 nm using a Cary 100 conc UV–vis Spectrophotometer Varian equipped with a diffuse reflectance attachment. Polytetrafluoroethylene was used as reference. TPR experiments were carried out in a Micromeritics AutoChem II 2920 automatic analyzer equipped with a TC detector. Before TPR experiments, the samples were pretreated *in situ* at 120 °C for 3 h under air flow and cooled in an Ar stream. The reduction step was performed under a stream of an Ar/H_2 mixture (90/10 mol/mol and 50 mL/min), with a heating rate of 10 °C/min up to 1000 °C. Carbon analysis was carried out using an automatic Perkin-Elmer 2400 Series II CHNS/O analyzer with TC detector. HRTEM measurements were performed using a Jeol 2010 microscope (resolving power 1.9 Å). The solids were ultrasonically dispersed in n-heptane and the suspension was collected on carbon coated grids. Slab length and layer stacking distributions of MoS_2 crystallites in each sample were established from the measurement of at least 300 crystallites detected on several HRTEM micrographs taken from different parts of the same sample dispersed on the microscope grid.

2.3. Catalytic activity

Prior to the catalytic activity testing, the catalysts were sulfided *ex situ* in a tubular reactor at 400 °C for 4 h in a stream of 15 vol.% of H_2S in H_2 under atmospheric pressure. The HDS activity tests were performed in a batch reactor at 300 °C and 7.3 MPa total pressure for 8 h with constant stirring. The sulfided catalysts (0.15 g) were transferred in an inert atmosphere (Ar) to a batch reactor (Parr) with 40 mL of n-hexadecane solution containing DBT (Aldrich) 1300 ppm of S. The course of the reaction was followed by withdrawing aliquots each hour and analyzing them on an HP-6890

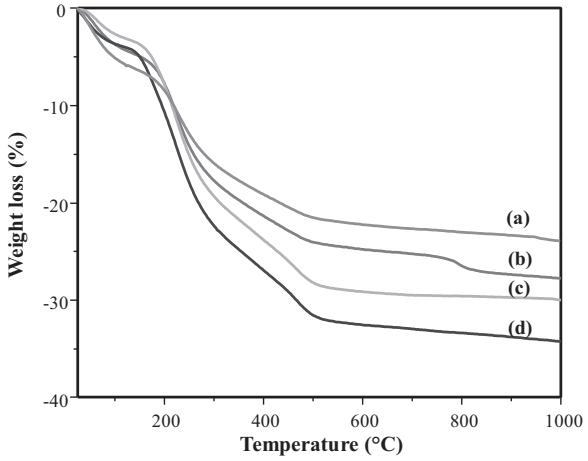

Fig. 1. Thermogravimetric analyses of (a) NiMoCA2.7, (b) NiMoCA4.2, (c) NiMoCA6.3 and (d) NiMoCA7.4 catalysts supported on SBA-15.

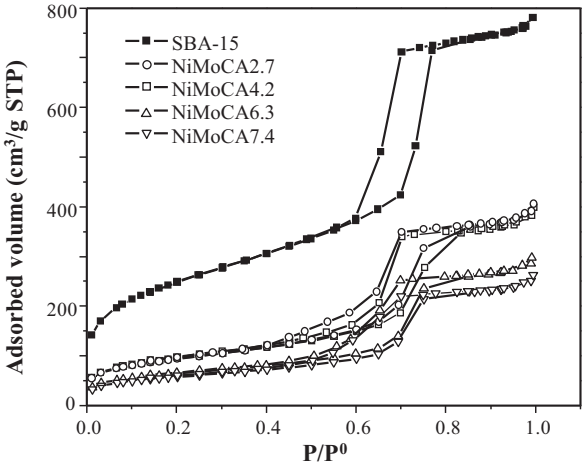

Fig. 2. Nitrogen adsorption–desorption isotherms of SBA-15 and NiMoCA(x) supported catalysts.

chromatograph. To corroborate product identification, the product mixture was analyzed on a Hewlett Packard GC MS instrument.

3. Results and discussion

3.1. Characterization of catalysts

TGA results under air atmosphere for NiMoCA(x) catalysts supported on SBA-15 are shown in Fig. 1. Weight loss at temperature about 120 °C or lower is attributed to water and ammonia desorption of physisorbed molecules on support. NiMoCA(x) catalysts showed the same profile for all of CA amounts. The CA decomposition by combustion in these materials under air atmosphere started at 200 °C and ended at 500 °C, a slope change at 150 °C indicated the onset of decomposition of CA. Weight loss magnitude is in good agreement with the CA charges deposited onto these materials, it increases with the CA amount: 24 wt.%, 27 wt.%, 29 wt.% and 33 wt.% for NiMoCA2.7, NiMoCA4.2, NiMoCA6.3, NiMoCA7.4 catalysts, respectively. According to TGA results, we studied the effect of CA amount in dried catalysts treated at 100 °C to conserve all of the CA content until sulfidation of these materials. The textural properties of SBA-15 and NiMoCA(x) catalysts are given in Table 1. SBA-15 specific surface area is 850 m^2/g, micropore area of 140 m^2/g and total pore volume of 1.09 cm^3/g. The impregnation of metal and CA species to the support resulted in a decrease of its textural properties. BET surface area decreases to 340 m^2/g, 338 m^2/g, 232 m^2/g and 207 m^2/g for NiMoCA2.7, NiMoCA4.2, NiMoCA6.3, NiMoCA7.4 catalysts, respectively; micropore area and total pore volume also decrease. These decrements in the textural properties are related with CA loading in the materials. The catalyst with the largest amount of CA has the less values in its textural properties. These results indicate that CA is adsorbed on SBA-15 surface proportionally to the amount of CA. Fig. 2 shows the adsorption-desorption isotherms of these materials. The characteristic shape of the SBA-15 isotherm (type IV isotherm with an H1 hysteresis loop) does not change by the impregnation of the metal and CA species. Only some decrease in the amount of adsorbed N_2 can be observed indicating that the original pore structure of the parent SBA-15 material is maintained after the impregnation step. A progressive decrease in the amount of the adsorbed N_2 is observed with the increase in CA loading. Small-angle XRD patterns of SBA-15 and NiMoCA(x) catalysts confirmed the *p6mm* pore structure conservation from support after the impregnation step. In Fig. 3, three reflections (d_{100}, d_{110} and d_{200}) characteristics for this pore symmetry are shown for all samples. However, the intensities of the three reflections of SBA-15 support decrease notably when CA loading is increased. Therefore, a slight decrease in long-range periodicity order of the support pores can be expected after CA incorporation, especially in the samples with high CA content. Results from the calculation of the pore wall thickness (δ) for the support and catalysts (last column, Table 1) confirm that CA loading on the NiMo/SBA-15 catalysts resulted in a small increase in the thickness of the pore walls of the starting SBA-15 support, this is probably related with the adsorption of CA on the SBA-15 surface. Powder XRD patterns of SBA-15 and NiMoCA(x) catalysts are shown in Fig. 4. The X-ray patterns of support and catalysts show a broad signal between 15° and 35°, which is attributed to the amorphous silica. No reflections were observed on NiMoCA(x) catalysts at various CA content, it indicates that metal species as well as CA are dispersed on SBA-15. The IR spectra of the support and NiMoCA(x) catalysts are shown in Fig. 5. The band at 1720 cm^{-1} is assigned to C=O stretching band. This vibration corresponds to the C=O bonds in the CA structure. It is important to note that C=O vibration intensity increased with the CA loading. This result is in good agreement with TGA, N_2 physisorption and small-angle XRD observations.

Electronic spectra of NiMoCA(x) catalysts in the range of 200–500 nm are shown in Fig. 6. The electronic transitions are assigned to ligand-to-metal charge transfer (LMCT) $O^{2-} \rightarrow Mo^{6+}$.

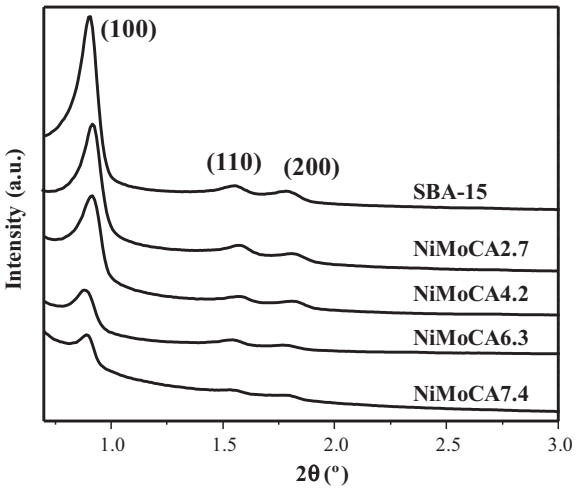

Fig. 3. Small-angle XRD patterns of SBA-15 and NiMoCA(x) supported catalysts.

Table 1
Textural characteristics of SBA-15 support and NiMoCA(x) catalysts.

Sample	S_{BET}[a] (m^2/g)	S_μ[b] (m^2/g)	V_p (cm^3/g)	V_μ (cm^3/g)	D_p[c] (Å)	a_o[d] (Å)	δ[e] (Å)
SBA-15	850	140	1.09	0.056	85	110	25
NiMo	613	108	0.84	0.043	80	111	31
NiMoCA2.7	340	64	0.62	0.026	76	112	36
NiMoCA4.2	338	50	0.61	0.019	75	112	37
NiMoCA6.3	232	34	0.46	0.013	74	113	39
NiMoCA7.4	207	28	0.40	0.011	73	114	41

[a] BET specific surface area.
[b] Micropore area estimated using the correlation of t-Harkins & Jura (t-plot method).
[c] Pore diameter corresponding to the maximum of the pore size distribution calculated from the adsorption isotherm by the BJH method.
[d] Unit-cell parameter estimated from the position of the (1 0 0) diffraction plane.
[e] Pore wall thickness ($\delta = a_o - D_p$).

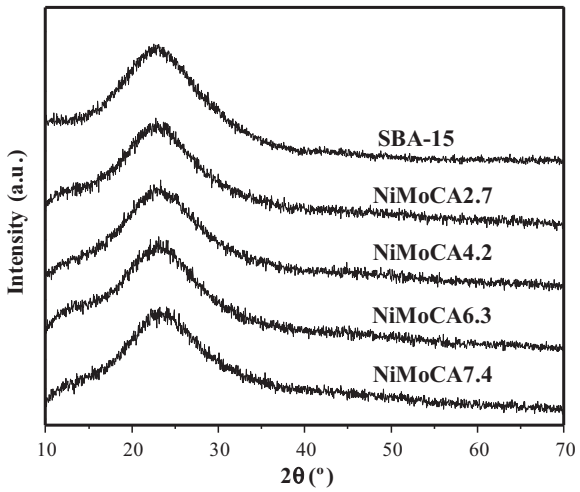

Fig. 4. Powder XRD patterns of SBA-15 and NiMoCA(x) supported catalysts.

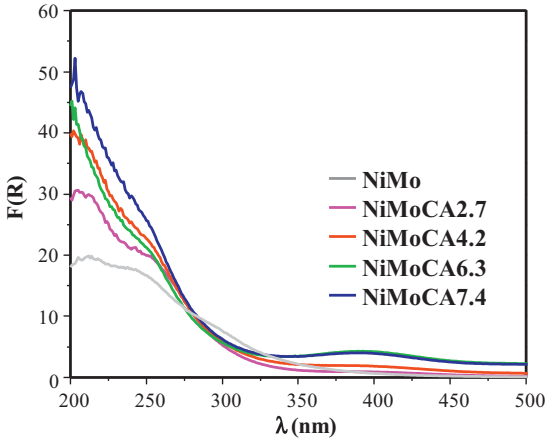

Fig. 6. UV–vis diffuse reflectance spectra of NiMoCA(x) catalysts supported on SBA-15.

It is well-known that the position of this LMCT band depends strongly on the local symmetry around the Mo^{6+} species and their aggregation state. The isolated molybdate species in tetrahedral coordination (Td) show a characteristic absorption band around 250 nm, whereas the signal of polymolybdate species in octahedral coordination (Oh) is observed at the 280–330 nm range and its position is affected by the aggregate size [32]. UV–vis absorption for NiMo catalyst without CA has a mixture of Mo oxide species in Td and Oh symmetry on SBA-15. DRS spectra of NiMoCA(x) catalysts supported on SBA-15 reveal the presence of a mixture of Mo^{6+} oxidic species in Td and Oh coordinations. A small band at 400 nm can be ascribed to a Ni–CA complex in Oh symmetry [33]. The spectra of these catalysts make evident the CA effect on dispersion of active phase. As CA loading is increased in the catalyst, a blue shift of the Mo absorption edge is observed reflecting an increase in the dispersion of Mo (Td) species.

TPR results for NiMoCA(x) catalysts supported on SBA-15 are shown in Fig. 7. The reduction profile of Mo with H_2 is dependent of the CA loading. NiMo/SBA-15 catalyst without CA shows hydrogen consumption in a broad temperature range (between 300 and 700 °C) with three main reduction peaks at 360, 467 and 663 °C. NiMoCA(x) catalysts also showed hydrogen consumption in a broad temperature range (between 300 and 700 °C). The main reduction

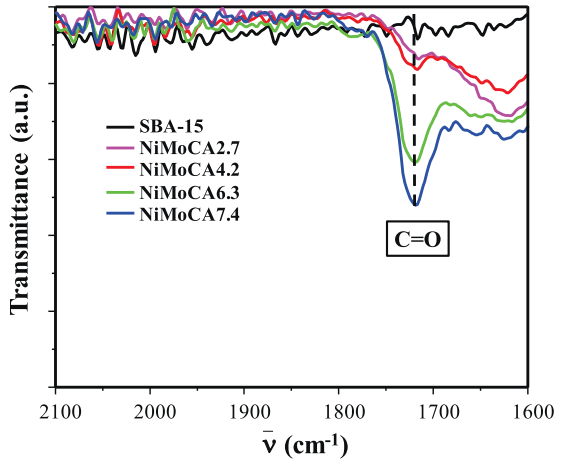

Fig. 5. FT-IR spectra of SBA-15 and NiMoCA(x) supported catalysts.

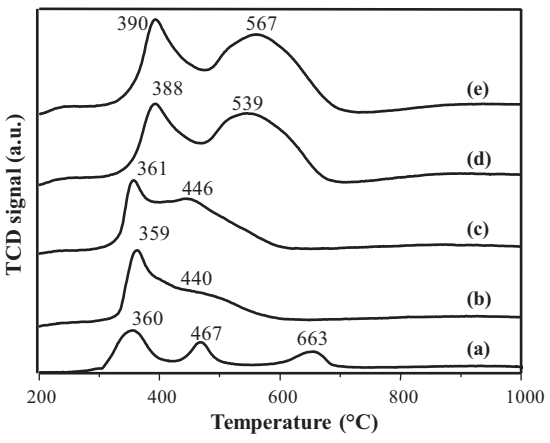

Fig. 7. TPR profiles of (a) NiMo, (b) NiMoCA2.7, (c) NiMoCA4.2, (d) NiMoCA6.3 and (e) NiMoCA7.4 catalysts supported on SBA-15.

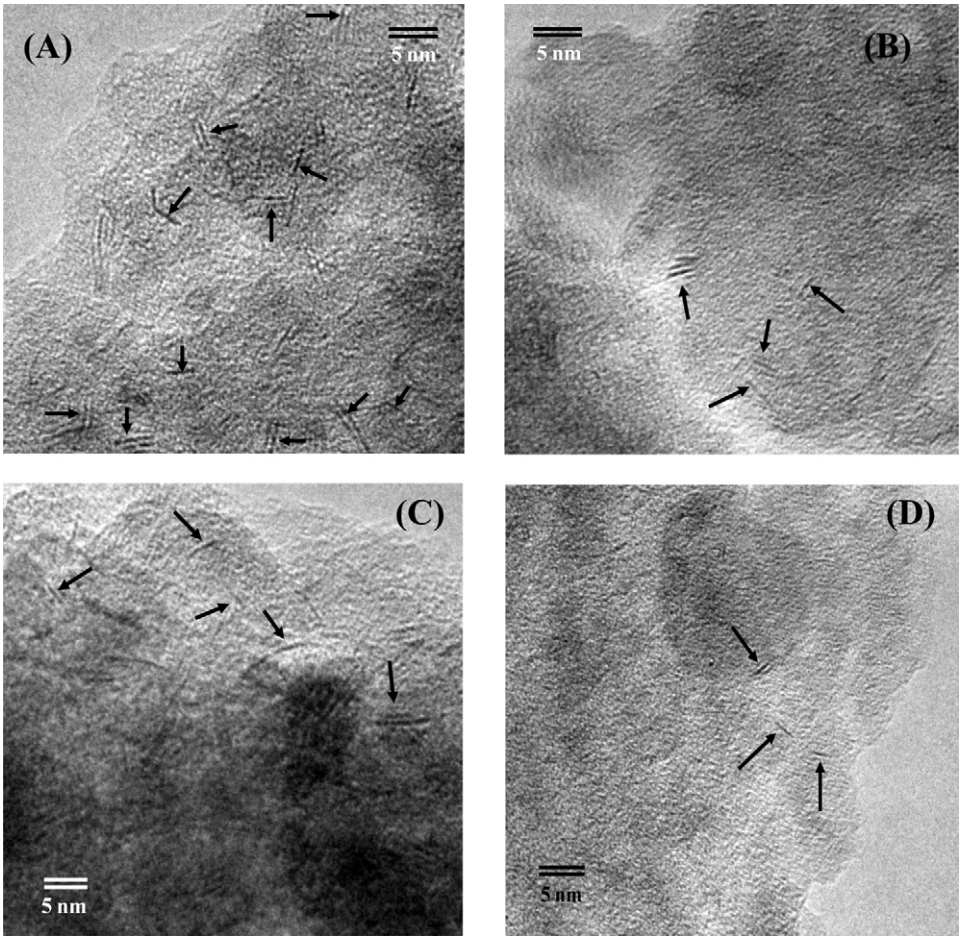

Fig. 8. HRTEM micrographs of sulfided catalysts: (A) NiMoCA2.7, (B) NiMoCA4.2, (C) NiMoCA6.3 and (D) NiMoCA7.4.

peaks of NiMoCA(x) catalysts can be attributed to the first step of Mo reduction ($Mo^{6+} + 2e^- \rightarrow Mo^{4+}$) of polymeric octahedral species weakly bound to the SBA-15 surface and the high temperature peak is associated with complete reduction ($Mo^{4+} + 4e^- \rightarrow Mo^0$) of polymeric octahedral, tetrahedral and bulk crystalline MoO_3 [34]. As CA content increases in SBA-15 the low temperature reduction peak shifts toward higher temperature along with gradual increase of peak area (from 359 °C for NiMoCA2.7 to 390 °C for NiMoCA7.4). The second reduction peak shifts toward higher temperature also along with gradual increase of peak area (from 440 °C for NiMoCA2.7 to 567 °C for NiMoCA7.4). Importantly, the second reduction peak is larger with the increasing of CA loading. It can indicate that a fraction of CA is reduced by its reaction with H_2. The H_2 consumption per gram of catalyst values in the TPR profile (Table 2) also supports this observation. The α factor is defined as volume consumed in the sample divided by theoretical volume to reduce completely Mo(VI) and Ni(II) species. The α factor is very high in the temperature range from 200 °C to 600 °C. NiMoCA4.2, NiMoCA6.3 and NiMoCA7.4 catalysts have α values higher than 1. It indicates that CA is reduced in the catalytic materials. We consider that the reducibility of CA under H_2 atmosphere needs special attention in the interpretation of the effect of this chelating agent in HDS catalysts. It is well-known that carboxylic acid functional group may be reduced. TPR experiments showed evidences of the CA reduction. To get a deeper insight into the effect of the CA reduction in these catalytic materials, carbon analysis was performed for sulfided catalysts. These experiments revealed that CA can act as a carbon source. The carbon content increases with the CA loading (Table 2).

Table 2
Hydrogen chemisorption, α factor and carbon content for NiMoCA(x) catalysts supported on SBA-15.

Catalyst	H_2 consumption (mL/g)	α (V/V_t)	C (wt.%)
NiMo	38	0.58	n.d.[a]
NiMoCA2.7	59	0.91	0.741
NiMoCA4.2	65	1.00	1.490
NiMoCA6.3	70	1.08	2.576
NiMoCA7.4	75	1.15	3.110

[a] Not determined.

HRTEM measurements of sulfided NiMoCA(x) catalysts were performed in order to gain more insight into the changes in the morphology and dispersion of active MoS_2 crystallites induced by the CA loading. Representative micrographs were selected for each of catalysts (Fig. 8), arrows note the MoS_2 crystallites at each micrograph. The typical fringes due to MoS_2 crystallites with 6.1 Å interplanar distances were observed on micrographs of all sulfided catalysts. The most important feature of these catalysts is the presence of a high proportion of low-stacked MoS_2 slabs formed by only one or two layers. Figs. 9 and 10 show the layer stacking and crystal length distributions of MoS_2 crystallites in sulfided catalysts supported on SBA-15 with different CA amount. The effect of increasing CA loading in NiMoCA(x) catalysts is clearly observed in the particle size distribution. The NiMoCA7.4 catalyst has a principal distribution around one and two layers and the particles length between 20–40 Å, whereas the NiMoCA2.7 catalyst showed larger MoS_2 particles. We note that the smallest particles were obtained in the catalysts prepared with the largest CA amount in impregnation solution. Average length and

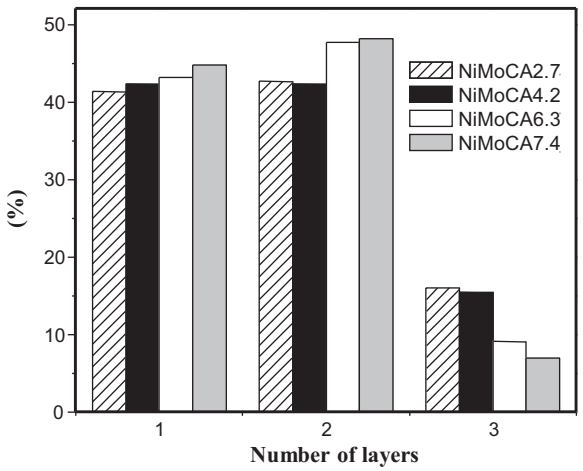

Fig. 9. Layer stacking distributions of MoS_2 crystallites in sulfided NiMoCA(x) catalysts supported on SBA-15.

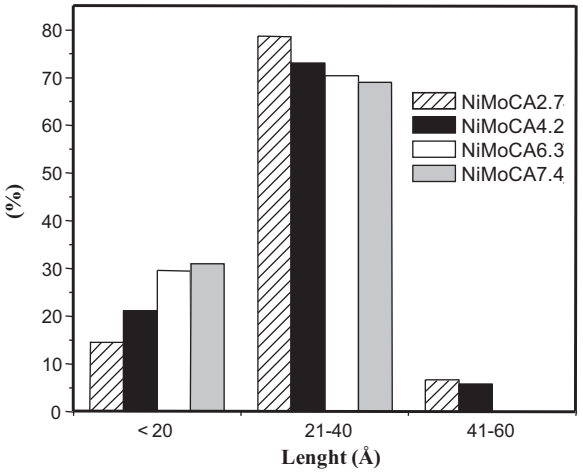

Fig. 10. Length distributions of MoS_2 crystallites in sulfided NiMoCA(x) catalysts supported on SBA-15.

Table 3
Average length, stacking degree and fraction of Mo atoms on the edge surface (f_{Mo}) of MoS_2 crystallites in NiMoCA(x) catalysts supported on SBA-15.

Catalyst	Average lenght (Å)	Average stacking	f_{Mo}
NiMo	45	3.9	0.26
NiMoCA2.7	28	1.8	0.40
NiMoCA4.2	26	1.8	0.43
NiMoCA6.3	22	1.6	0.49
NiMoCA7.4	20	1.5	0.53

stacking degree of MoS_2 particles observed in NiMoCA(x) sulfided catalysts are shown in Table 3. As we discussed above, the CA amount added in the impregnation solution decreased the size of MoS_2 active phase. The largest values were obtained for NiMoCA2.7 catalyst (length of 28 Å and stacking degree of 1.8) and the smallest values for NiMoCA7.4 catalyst (length of 20 Å and stacking degree of 1.5).

The average fraction of Mo atoms on the edge surface (f_{Mo}) of MoS_2 crystallites is a dispersion index of the active phase in NiMoCA(x) supported catalysts. It was calculated with morphology data from HRTEM measurements based on geometrical considerations assuming that this MoS_2 slabs are perfect hexagons [35]. The f_{Mo} for NiMoCA(x) catalysts are reported in Table 3.

3.2. Catalytic activity

Dibenzothiophene hydrodesulfurization was performed for the NiMoCA(x) catalysts synthesized and characterized as here above described to evaluate the effect of CA loading in HDS. This S-containing aromatic molecule was selected because it is representative of gasoline and diesel fuels and may react quantitatively by the two sulfur elimination routes of aromatic compounds such as hydrogenation (HYD), aromatic rings react with H_2 to saturate C=C aromatic bonds, and direct desulfurization (DDS), hydrogenolysis (HYG) reaction breaks C–S bond without pre-hydrogenation of aromatic rings. A general reaction network for DBT [36] is shown in Fig. 11. The major preference of DBT reaction in its network is dependent of some HDS conditions, in special the nature of the catalyst, such as support composition, active phase, promoter or additive [5,27,37,38].

The DBT conversions at 4 and 8 h obtained over NiMoCA(x) catalysts supported on SBA-15 are shown in Table 4. The conversion of DBT decreased when the CA content increased. The overall pseudo-first order rate constants (k) and initial reaction rates (r_o) are also shown in Table 4. These kinetic parameters are in the same direction than conversion. NiMoCA2.7 catalyst has the highest rate constant $3.56 \times 10^{-4}\ s^{-1}\ g_{cat}{}^{-1}$ and the lowest one is $2.62 \times 10^{-4}\ s^{-1}\ g_{cat}{}^{-1}$ for NiMoCA7.4 catalyst. The increment in the CA loading decreases the activity of these catalysts. However, the catalytic activity for all of these NiMo/SBA-15 catalysts prepared with CA is higher than the catalyst prepared without CA. Selectivity modifications by CA loading in NiMo catalysts supported on SBA-15 were studied by the composition of products. Outstanding modifications were observed along DBT conversion (Fig. 12). Really surprising selectivity modifications were obtained by varying the amount of CA in the catalysts. The DDS route is preferred when the CA is increased in aqueous solutions. The thermodynamic stability of DBT to react through HYD route is larger than its DDS counterpart [39], the selectivity preference of these catalysts could explain the activity observed. Table 5 contains the rate constants which were calculated based on the kinetic model proposed by Farag [40,41]. This model is based on the assumption of the existence of two different kinds of catalytic active sites of (i) hydrogenation and (ii) direct desulfurization. The solved differential equations to calculate the rate constants are:

$$C_{DBT} = C_{DBT^o}\ \exp(-k_0 t) \quad (1)$$

$$C_{BP} = \frac{C_{DBT^o} k_1^*}{k_3^* - k_0}[\exp(-k_0 t) - \exp(-k_3^* t)] \quad (2)$$

Table 4
Conversion of DBT at 4 and 8 h over NiMoCA(x) catalysts supported on SBA-15, overall pseudo-first order rate constant (k) and initial reaction rate (r_o).

Catalyst	DBT conversion (%)		k, $\times 10^4$ ($s^{-1}\ g_{cat}{}^{-1}$)	r_o, $\times 10^2$ ($mol\ L^{-1}\ h^{-1}\ g_{cat}{}^{-1}$)
	4 h	8 h		
NiMo	36	72	2.40	1.95
NiMoCA2.7	50	91	3.56	2.79
NiMoCA4.2	46	87	3.22	2.51
NiMoCA6.3	42	84	2.81	2.30
NiMoCA7.4	39	80	2.62	2.17

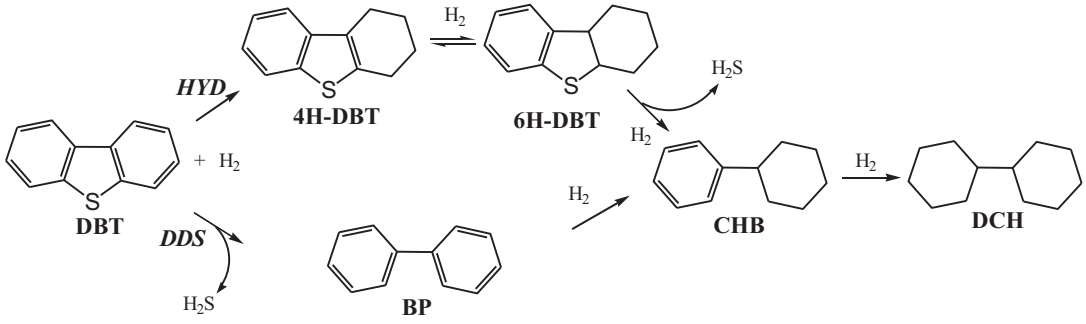

Fig. 11. Reaction network for hydrodesulfurization of dibenzothiophene. DBT = dibenzothiophene; 4H-DBT = tetrahydrodibenzothiophene; 6H-DBT = hexahydrodibenzothiophene; BP = biphenyl; CHB = cyclohexylbenzene; DCH = dicyclohexyl.

$$C_{CHB} = \frac{C_{DBT^o} k_3^* k_1^*}{k_3^* - k_1^*} \left[\frac{1}{k_3^*} \exp(k_3^* t) - \frac{1}{k_0} \exp(k_0 t) \right] + \frac{C_{DBT^o} k_4^* k_2^*}{k_4^* - k_0} \left[\frac{1}{k_4^*} \exp(k_4^* t) - \frac{1}{k_0} \exp(k_0 t) \right] + \frac{C_{DBT^o}(k_1^* + k_2^*)}{k_0} \quad (3)$$

where $k_0 = k_1 K_1 + k_2 K_2$, k_1 and k_2 are the intrinsic kinetic rate constants for the DDS and HYD routes, and K_1 and K_2 are the equilibrium adsorption constants of DBT over the catalytic active sites for DDS and HYD, respectively. All of these constants are lumped together as one constant, i.e., k_0 (the overall pseudo-first order rate constant reported in Table 4). The apparent rate constants adjusted were $k_n^* = k_n K_n$, where k_n is the intrinsic kinetic rate constant and K_n is the equilibrium adsorption constant of each compound.

We described the calculation of these constants in our previous work using Origin 8.0 software [27]. The rate constants k_1^* (DBT → BP) and k_4^* (4H-DBT → CHB) are related to hydrogenolysis reactions and k_2^* (DBT → 4H-DBT) and k_3^* (BP → CHB) correspond to hydrogenation reactions of DBT and its HDS products. The rate constants decrease with the CA loading as a consequence of the smaller values of the overall pseudo-first order rate constant. DBT

Table 5
Apparent rate constants of NiMoCA(x) catalysts for HDS of DBT in its reaction network.

Catalyst	Rate constants, $\times 10^4$ s^{-1} g$_{cat}^{-1}$				Ratio	
	k_1^*	k_2^*	k_3^*	k_4^*	$\frac{k_1^*}{k_2^*}$	$\frac{k_4^*}{k_3^*}$
NiMo	1.05	1.35	3.65	3.50	0.78	0.96
NiMoCA2.7	3.03	0.67	0.90	8.67	4.51	9.63
NiMoCA4.2	2.87	0.39	0.70	8.12	7.36	11.60
NiMoCA6.3	2.70	0.19	0.33	7.72	14.21	23.39
NiMoCA7.4	2.51	0.12	0.27	7.53	20.92	27.89

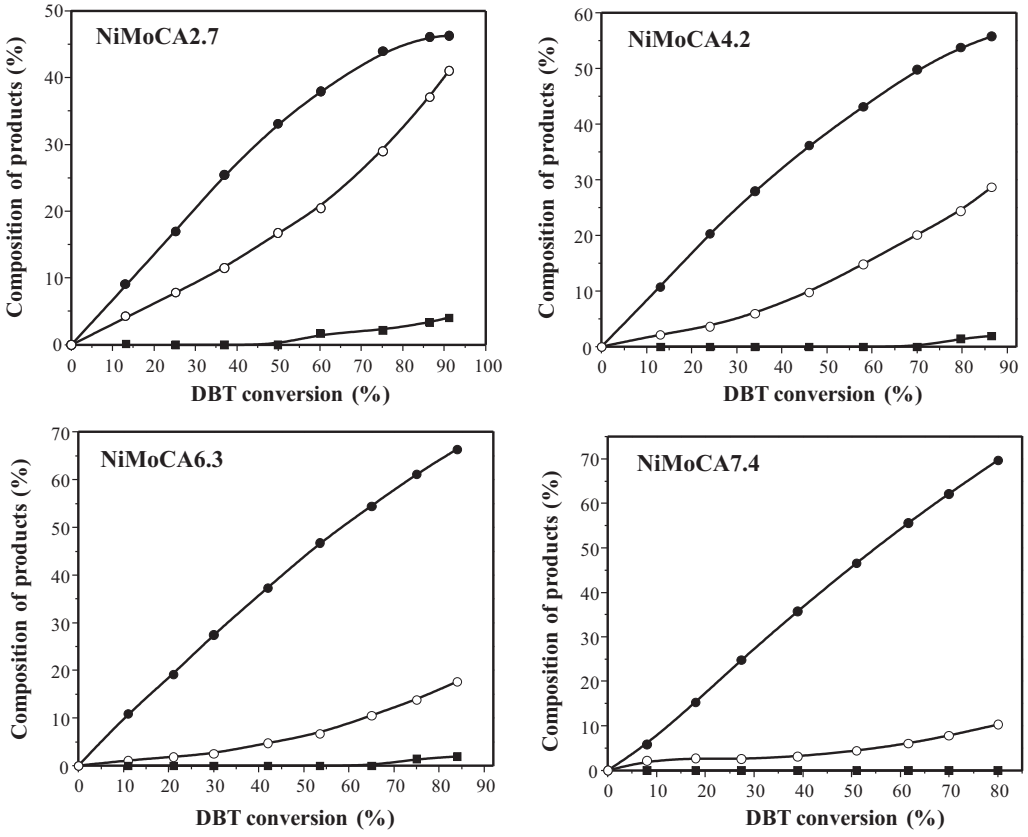

Fig. 12. Composition of products along with conversion in HDS of DBT. Products detected in HDS were: (●) biphenyl (BP), (○) cyclohexylbenzene (CHB) and (■) dicyclohexyl (DCH).

reacts over the catalyst without CA toward HYD route as we can see $k_1^*/k_2^* = 0.78$ and $k_4^*/k_3^* = 0.96$. The amount of CA added in these catalysts change the ratio of HDS routes. The ratio between HYG and HYD rate constants is larger when CA loading increases. The NiMoCA7.3 catalyst has the largest selectivity in HDS of DBT through HYG reactions $k_1^*/k_2^* = 20.92$ and $k_4^*/k_3^* = 27.89$. CA provides a change in the population of catalytically active sites to these materials [27]. As it has been reported, the preferential adsorption of the aromatic compounds on the HYD sites (Mo-edge brim sites) could be responsible for the selective inhibition of the HYD route in the HDS of DBT [42]. We observed that the CA incorporates carbon in the catalytic materials. The carbon content in these catalysts is related to the amount of CA added in the impregnation solutions. It could be possible that the carbon deposited on these materials has an aromatic character. Furthermore, the observed effect is in good agreement with the increasing amount of this element in sulfided catalysts.

CA addition in the impregnation solution of NiMo/SBA-15 catalysts for HDS has several implications in all of the preparation steps. In this line, the effect of CA has been ascribed to the formation of complexes with metal species in solution [43]. We consider this effect is important, but not the main reason of the beneficial effect in the activity of these catalysts. CA added alters the chemical equilibrium of Mo(VI) in aqueous solution [44]. The species impregnated to the support were not the same than the typical heptamolybdate. On the other hand, the properties of catalytic materials have also modifications due to CA addition. The CA adsorbed on the surface of SBA-15 modifies this support, when the catalysts are activated under reducing atmosphere the CA reacts to form carbon, as we observed in TPR experiments. CA acts as a carbon source, as we detected in the composition of the catalytic materials. The CA in the aqueous solutions leaves carbon after sulfidation stage. The incorporation of carbon on the SBA-15 has consequences in the interaction between the support and the MoS_2 active phase, the morphology of catalytic particles was modified due to CA loading. The average length and stacking degree of MoS_2 particles are also related to the DBT selectivity over these catalysts when CA was added.

We consider these drastic changes in selectivity by CA loading in NiMoCA(x) catalysts have not been reported previously. We believe that CA and SBA-15 for NiMo catalysts are the responsible of these outstanding results because other studies, where the CA amount was varied, did not observe any selectivity changes [24]. The DDS route preference of DBT over these catalysts is related to the carbon content. However, the function of CA is not only leaving carbon, the properties discussed above become this organic acid an attractive additive to synthesize HDS catalysts supported on SBA-15. The DDS promotion with CA is easy to handle and the activity is not decreased drastically as it has been reported for catalysts supported on SBA-15 modified with basic oxides [45]. Furthermore, the use of CA in these catalytic materials provides a good option to reduce de hydrogen consumption in the sulfur elimination from the S-containing compounds which can react toward this route.

4. Conclusions

NiMo catalysts supported on SBA-15 were synthesized with citric acid. Some changes were observed by the CA addition in their properties. The use of CA during impregnation of metal species to support has several consequences. The amount of CA modifies the textural properties. TPR results showed the reduction of some parts of CA under reducing atmosphere. Carbon analysis reveals this reduction leaving traces of this element in the sulfided catalysts. The amount of carbon increases with the CA loading. The incorporation of carbon on these materials results in modification of the morphology of MoS_2 particles.

Catalytic activity exhibited an increase for the CA addition compared with NiMo/SBA-15 catalyst without CA. However, the large CA amount decreases the catalytic activity. We noted outstanding promotion of DDS route related to the CA loading. This effect provided by CA has not been reported previously. DBT reacts toward DDS route over these catalysts with a surprising selectivity without considerable abatement in the sulfur elimination. We showed that population of HYD and DDS catalytic sites changes with the CA loading in the catalysts. Furthermore, these catalytic materials have some advantages in the promotion of hydrogenolysis reactions.

Acknowledgements

Financial support by CONACyT-Mexico (grant 100945) is gratefully acknowledged. D.V. acknowledges to CONACyT (32251/207815), as well as L. Peña and R. Olivares-Amaya for insightful discussions. The authors thank M. Portilla, E. Reynoso, C. Salcedo Luna, M. Aguilar, V.H. Lemus, N. López and I. Puente Lee for technical assistance with TGA, small-angle and powder XRD, elemental analysis and electron microscopy characterizations, respectively.

References

[1] http://www.dieselnet.com/standards/fuels.html.
[2] U.T. Turaga, C. Song, Catalysis Today 86 (2003) 129–140.
[3] A. Wang, Y. Wang, T. Kabe, Y. Chen, A. Ishihara, W. Qiany, Journal of Catalysis 199 (2001) 19–29.
[4] O.Y. Gutiérrez, D. Valencia, G.A. Fuentes, T. Klimova, Journal of Catalysis 249 (2007) 140–153.
[5] D. Valencia, T. Klimova, Catalysis Today 166 (2011) 91–101.
[6] R. Nava, R.A. Ortega, G. Alonso, C. Ornelas, B. Pawelec, J.L.G. Fierro, Catalysis Today 127 (2007) 70–84.
[7] S. Garg, K. Soni, G.M. Kumaran, M. Kumar, J.K. Gupta, L.D. Sharma, G.M. Dhar, Catalysis Today 130 (2008) 302–308.
[8] R. Cattaneo, T. Shido, R. Prins, Journal of Catalysis 185 (1999) 199–212.
[9] T. Shimizu, K. Hiroshima, T. Honma, T. Mochizuki, M. Yamada, Catalysis Today 45 (1998) 271–276.
[10] G. Kishan, L. Coulier, V.H.J. de Beer, J.A.R. van Veen, J.W. Niemantsverdriet, Chemical Communications 13 (2000) 1103–1104.
[11] M. Che, O. Clause, C. Marcilly, in: G. Ertl, H. Knözinger, J. Weitkamp (Eds.), Preparation of Solid Catalysts, Wiley-VCH, 1999, pp. 315–340, chapter 4.1.1.
[12] A.J. van Dillen, R.J.A.M. Terörde, D.J. Lensveld, J.W. Geus, K.P. de Jong, Journal of Catalysis 216 (2003) 257–264.
[13] S. Boujday, J.-F. Lambert, M. Che, Journal of Physical Chemistry B 107 (2003) 651–654.
[14] J.-F. Lambert, M. Hoogland, M. Che, Journal of Physical Chemistry B 101 (1997) 10347–10355.
[15] Y. Sung, J.C. Park, B. Lee, Y. Kim, J. Yi, Catalysis Letters 81 (2002) 89–96.
[16] L. Espinosa-Alonso, K.P. de Jong, B.M. Weckhuysen, Journal of Physical Chemistry C 112 (2008) 7201–7209.
[17] M.A. Lélias, P.J. Kooyman, L. Mariey, L. Oliviero, A. Travert, J. van Gestel, J.A.R. van Veen, F. Maugé, Journal of Catalysis 267 (2009) 14–23.
[18] M.S. Rana, J. Ramírez, A. Gutiérrez-Alejandre, J. Ancheyta, L. Cedeño, S.K. Maity, Journal of Catalysis 246 (2007) 100–108.
[19] O.V. Klimov, A.V. Pashigreva, M.A. Fedotov, D.I. Kochubey, Y.A. Chesalov, G.A. Bukhtiyarova, A.S. Noskov, Journal of Molecular Catalysis A: Chemical 322 (2010) 80–89.
[20] T. Fujikawa, Topics in Catalysis 52 (2009) 872–879.
[21] T. Fujikawa, M. Kato, T. Ebihara, K. Hagiwara, T. Kubota, Y. Okamoto, Journal of the Japan Petroleum Institute 48 (2005) 114–120.
[22] T. Fujikawa, H. Kimura, K. Kiriyama, K. Hagiwara, Catalysis Today 111 (2006) 188–193.
[23] T. Fujikawa, M. Kato, T. Ebihara, K. Hagiwara, T. Kubota, Y. Okamoto, Journal of the Japan Petroleum Institute 48 (2005) 106–113.
[24] J. Escobar, M.C. Barrera, J.A. de los Reyes, J.A. Toledo, V. Santes, J.A. Colín, Journal of Molecular Catalysis A: Chemical 287 (2008) 33–40.
[25] H. Li, M. Li, Y. Chu, F. Liu, H. Nie, Applied Catalysis A 403 (2011) 75–82.
[26] A. Tuxen, H. Gøbel, B. Hinnemann, Z. Li, K.G. Knudsen, H. Topsøe, J.V. Lauritsen, F. Besenbacher, Journal of Catalysis 281 (2011) 345–351.
[27] D. Valencia, T. Klimova, Catalysis Communications 21 (2012) 77–81.
[28] D. Zhao, J. Feng, Q. Huo, N. Melosh, G.H. Fredrickson, B.F. Chmelka, G.D. Stucky, Science 279 (1998) 548–552.
[29] D. Zhao, Q. Huo, J. Feng, B.F. Chmelka, G.D. Stucky, Journal of the American Chemical Society 120 (1998) 6024–6036.

[30] D. Valencia, I. García-Cruz, T. Klimova, Studies in Surface Science and Catalysis 175 (2010) 529–532.
[31] T. Yamada, H. Zhou, K. Asai, I. Honma, Materials Letters 56 (2002) 93–96.
[32] R.S. Weber, Journal of Catalysis 151 (1995) 470–474.
[33] C. Lepetit, M. Che, Journal of Physical Chemistry 100 (1996) 3137–3143.
[34] R. López Cordero, A. López Agudo, Applied Catalysis A 202 (2000) 23–35.
[35] E.J.M. Hensen, P.J. Kooyman, Y. van der Meer, A.M. van der Kraan, V.H.J. de Beer, J.A.R. van Veen, R.A. van Santen, Journal of Catalysis 199 (2001) 224–235.
[36] M.J. Girgis, B.C. Gates, Industrial and Engineering Chemistry Research 30 (1991) 2021–2058.
[37] H. Wang, R. Prins, Journal of Catalysis 264 (2009) 31–43.
[38] Y. Sun, R. Prins, Journal of Catalysis 267 (2009) 193–201.
[39] D. Valencia, L. Peña, I. García-Cruz, International Journal of Quantum Chemistry (2012), http://dx.doi.org/10.1002/qua.24242.
[40] H. Farag, Energy and Fuels 20 (2006) 1815–1821.
[41] H. Farag, Journal of Colloid and Interface Science 348 (2010) 219–226.
[42] A. Stanislaus, A. Marafi, M.S. Rana, Catalysis Today 153 (2010) 1–68.
[43] A.V. Pashigreva, O.V. Klimov, G.A. Bukhtiyarova, M.A. Fedotov, D.I. Kochubey, Yu.A. Chesalov, V.I. Zaikovskii, I.P. Prosvirin, A.S. Noskov, Studies in Surface Science and Catalysis 175 (2010) 109–116.
[44] R.I. Maksimovskaya, G.M. Maksimov, Inorganic Chemistry 46 (2007) 3688–3695.
[45] T. Klimova, L. Peña, L. Lizama, C. Salcedo, O.Y. Gutiérrez, Industrial and Engineering Chemistry Research 48 (2009) 1126–1133.